Partial-gross slip fretting transition of martensitic stainless steels

Partial-gross slip fretting transition of martensitic stainless steels

M. Lavella*
Department of Mechanical and Aerospace Engineering, Politecnico di Torino Corso Duca degli Abruzzi, 24-10129 Torino – Italy

Abstract

Based on critical reviews of the well-known dependence of fretting process upon the sliding amplitude, experiments were performed to verify this dependence. One of the main critical points is that the experiments which led to this result were performed controlling the imposed displacement amplitude instead of the real sliding amplitude. Therefore, the difference between the real displacement amplitude and the imposed amplitude due to compliances of the test rigs components was not considered. Fretting tests were performed using a high precision test rig. One of the main peculiarities of this test rig is that there is no difference between the imposed sliding amplitude and the real amplitude. The fretting process parameters of experiments were room temperature, two normal load (contact pressure 15, 25 MPa), four strokes (10, 15, 20, 50 micrometres), two martensitic stainless steels (X20Cr13, M152) and different durations from 15 to 160 M-cycles. Friction coefficient was computed using the hysteresis loops measured during the wear test. The worn surfaces were measured using an optical instrument based on focus variation. Wear volumes were accurately computed with a procedure that takes in to account the roughness of the surfaces. Results show that the friction coefficient is independent of slip amplitude, normal load and steel type if the hysteresis loops shape is parallelogrammatic and the contact surfaces are effectively conformal. When these conditions are not observed, the friction coefficient is dependent on normal load, even in contrast with its increase. Wear volume shows linear evolution in gross slip regime while it is non-linear in partial slip. Wear rate is independent of slip amplitude and normal load in partial slip regime at low ratio amplitude contact length. In contrast, wear rate depends on slip amplitude and exhibits a sharp increase near the transition partial-gross slip.

Keywords: Fretting regimes, martensitic stainless steels, X20Cr13, M152.

*Corresponding author. Tel.: +39 011 0906935; fax: +39 011 0906999.
E-mail address: mario.lavella@polito.it (Mario Lavella)

1. Introduction

The term fretting refers to the damage process of contact mating surfaces subject to reciprocating relative motion of low amplitude. Fretting degradation simultaneously involves fatigue, wear and oxidation. This phenomenon was first reported by [1] who found oxidized debris generated at contact interfaces of grip-specimens of their fatigue test machines [2]. The first published study focused on fretting is reported in [3]. Subsequently, a large body of literature has been disseminated for a wide range of engineering applications. The reason is that the fretting degradation process can be found near all mechanical components dynamically loaded with a friction-based joint. Some of the most studied joints subject to fretting degradation are the contact surfaces of turbine blades, particularly the contact interfaces blades-disk [4], [5], blade-blade and blade-damper [6]. Fretting is one of the most important causes of in-service damage of turbines [7]. In this case, the relative motion of low amplitude comes from the blade vibration. Even if many studies focused on the mitigation/control of the blade vibration are available in literature, the dynamic response of the blades is strictly related with energy dissipated by contact surfaces [8]-[10]. Consequently, the degradation due to the fretting of these interfaces plays a primary role in blade dynamics.

Fretting degradation mechanisms depend on process parameters, materials and environmental conditions. In order to describe the behavior of the mating surface, maps are commonly constructed. These maps are diagrams that summarize the damage rate (wear rate and fatigue damage are common) as a function of the specific regime and/or degradation mechanism for a given set of process parameters. The application of this methodology to fretting processes can be found [11] while [12] reports an application to wear of steels. Depending on the focus of the analysis, different maps can be constructed. The map wear rate as a function of stroke or displacement amplitude with the evidence of fretting regimes is one of the most important maps. The reason is that wear and fatigue damage rate are strongly dependent on displacement amplitude. A very famous fretting map in terms of fretting damage and amplitude is reported in [11]. This map is qualitatively reconstructed in Fig. 1 (a) as proposed in [11]. It reports the fatigue life and the wear rate K’ (wear volume normalized with respect to the normal load and sliding distance) as a function of displacement amplitude with the evidence of the fretting regimes *stick*, *mixed stick-slip*, *gross slip* and *reciprocating*. In [11], the first three fretting

regimes are distinguished based on the hysteresis loop, tangential contact force as a function of relative displacement. The characteristic loop and the sliding condition of the contact mating surfaces of these regimes are reported in Fig. 2. If p_1, p_2 . . .p_n . . . p_N are the contact points of the mating surfaces, in stick regime all points are in stick condition, in mixed stick-slip regime a part of the points is in slip and the complementary part is in stick while in the gross slip regime all points are in sliding. The localization of stick points depends on the contact geometry [13], e.g. they are at the center of contact area for sphere – on – flat contacts. The fourth regime is called *reciprocating sliding regime*. This is the limit of the fretting degradation process and it comes when the sliding amplitude is higher than 300 μm [11]. If the reciprocating sliding amplitude is higher than this limit, wear mechanism and wear rate are the same as that found in unidirectional sliding. The map of Fig. **1** (a) indicates that the wear rate increases sharply in stick and gross slip regimes while it shows a mild increase or remains approximately constant in mixed stick-slip and reciprocating regimes.

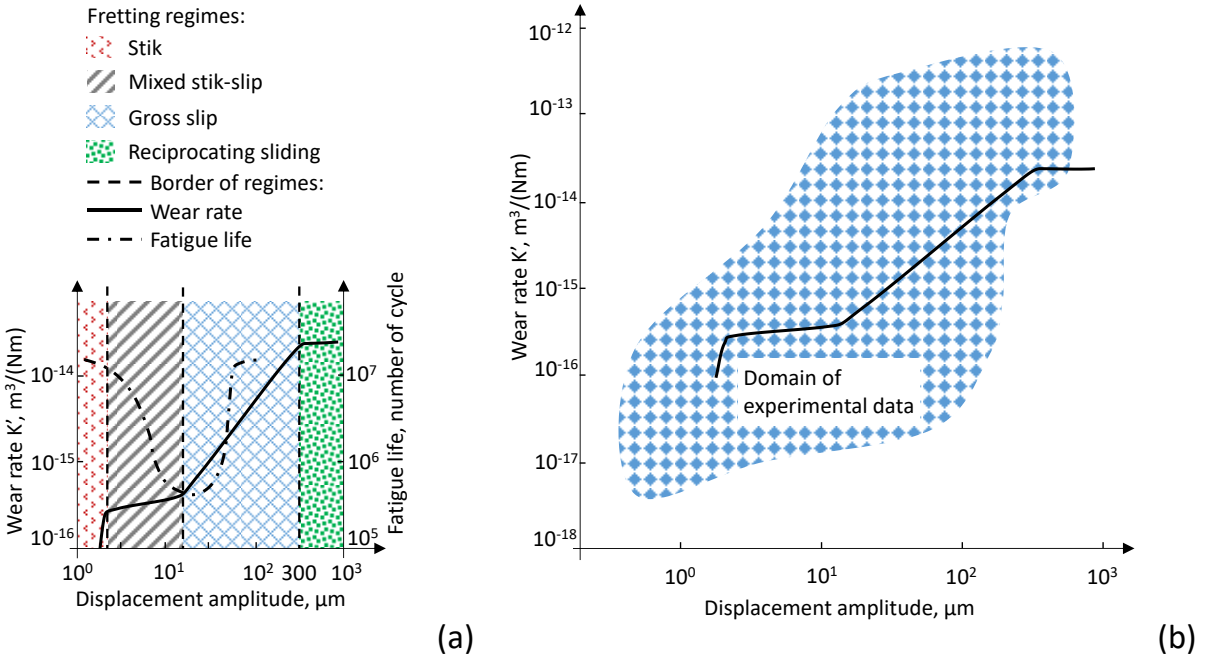

Fig. 1 Qualitative fretting maps with the evidence of fretting regime: (a) map wear rate and fatigue damage as a function of displacement amplitude, qualitative reconstruction from [11]; (b) Same wear map (a) with the evidence of the experimental data, qualitative reconstruction from [15], [16].

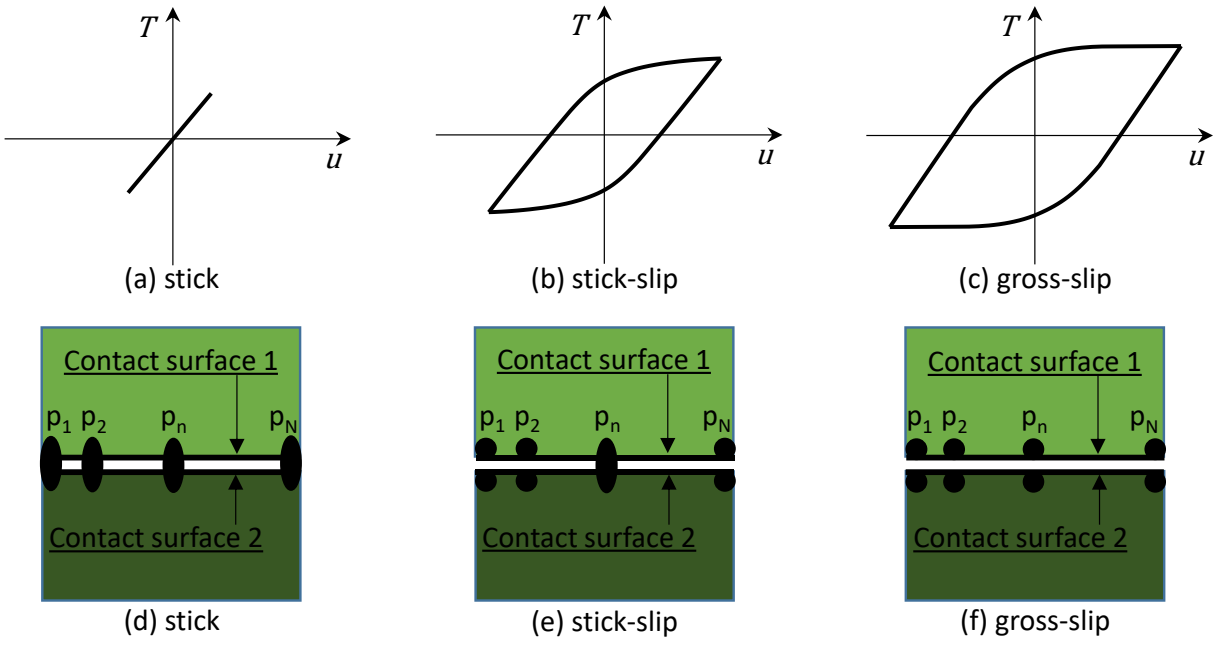

Fig. 2 (a, b, c) Characteristic aspect of hysteresis loop for different fretting regimes [11], stick (a), mixed stick-slip (b), and gross slip (c); (d, e, f) sliding state of the mating surfaces, (d) stick in the whole contact interface, (e) part of the contact interface in slip and the complementary part in stick, (f) slip in the whole contact interface.

Fatigue life shows a minimum in proximity of the border of mixed stick-slip and gross slip regimes. This effect seems to be coherent with a competition between wear and crack propagation. Wear inhibits fatigue crack propagation by removing a layer of material. Consequently, a new crack nucleation could also be necessary. On the other hand, in mild wear condition, fatigue crack propagation is faster than the material layer removal by wear. Moreover, by modelling analysis have been also found that wear increases contact area which reduces stress [14].

The trend of the wear rate on the sliding amplitude reported in [11], Fig. **1** (a), has been critically reviewed [15] [16]. The necessity for further study comes from the strong dispersion of the experimental data used to construct the map in Fig. 1 (a). These experimental data came from the literature and were not reported in [11]. In [15], the same wear rate map as in Fig. 1 (a) was constructed including the experimental data. This second map made evident the high level of data dispersion. In order to qualitatively illustrate the level of the dispersion, the map in Fig. 1 (a) was reconstructed in Fig. 1 (b) including the domain of experimental data. This strong data dispersion motivates further studies. Excluding the obvious differences due to the different

procedures used, the data dispersion has been attributed to the difference between the imposed sliding amplitude and the real sliding amplitude of the fretting process [16]. The problem is that the sliding amplitude is not commonly measured in proximity of the sliding surface. Usually displacement transducer such as LVDT (Linear Variable Differential Transformer) are used to measure the displacement in a position that is linked to the contact surfaces by means of test rig components. For example the sliding amplitude is measured where it is imposed and not in proximity of the contact surfaces. Consequently, between the contact surfaces and the amplitude measurements point there is one or more test rig components with a specific compliance. In other words, during the fretting process the imposed sliding amplitude is commonly measured and controlled instead of the real relative sliding amplitude of the mating surfaces. The problem is that the measurements of imposed sliding amplitude also include the compliances of test rig components between the measurement point and the contact surface. These strains cannot be neglected because of the low amplitude of the fretting process. An analysis of the effects of this compliance is reported in [17]. The displacement measurements when the tangential force is zero [5] is a good strategy to reduce the compliance effects in the amplitude measurements. In this condiction, there are no static loads on the exciting apparatus of the test rig. However, this strategy does not provide a precise displacement control during the whole load cycle.

The present research aims to investigate the dependence of the fretting process upon the sliding amplitude, without the problems due to the difference between imposed and real displacement amplitude. Experiments were performed in order to verify the dependence of fretting process upon the slip amplitude. The high precision test rig in [18], [19] was used for the fretting tests. The main peculiarities of this test rig are flat on flat contact with free approaching of contact surfaces; real displacement control in proximity of the contact surfaces; contact force and relative displacement measured continuously for each hysteresis loop; working temperature from room temperature to more than 1000 °C. The relative displacement is measured very close to the contact interfaces. Substantially there is no difference between the imposed and real sliding amplitude of the mating surfaces. In other words, the compliance of test rig components have no effect on the displacement measurements. Moreover, because of the free approach and the characteristics of the specimen fixture, the test rig allows the disassembling and subsequent re-assembling with a negligible impact on the fretting process. Disassembling – assembling operations are necessary to measure the 3D profile of the worn surfaces and to evaluate the wear

volume. A great advantage of this rig is that wear volume measurements can be performed on the same couple of specimens at different stages of the fretting process. Experiments were performed at room temperature, two contact pressures (15, 25 MPa), four strokes (10, 15, 20, 50 micrometres), two martensitic stainless steels (X20Cr13, M152) and different durations from 15 to 160 M-cycles. These materials and process parameters are typical in the joints of steam turbines blades at low-pressure stages. An evaluation of the effects of low temperature variation, normal load, heat treatment and surface integrity at constant stroke for the same steels can be found in [6]. In the present research, the focus is on the effects of the sliding amplitude. Friction coefficient was computed using the hysteresis loops measured during the wear test. The worn surfaces were measured by optical instrument based on focus variation. Wear volumes were accurately computed with a procedure that takes into account the roughness of the surfaces [20]. This procedure is fundamental in order to evaluate the mild wear volumes at low amplitude.

Results show that the friction coefficient is more dependent on the shape of the hysteresis loops than on slip amplitude, normal load and steel type. Moreover, the friction coefficient is independent of slip amplitude, normal load and steel type if the hysteresis loops shape is parallelogrammatic and the contact surfaces are effectively conformal. When these conditions are not observed, the friction coefficient is dependent on the normal load, even in contrast with its increase. Wear volume shows linear evolution in gross slip regime while it is non linear in partial slip. The non-linearity ends when the wear scar covers the full contact length. Wear rate is independent of slip amplitude and normal load in partial slip at low ratio amplitude - contact length. In contrast, wear rate depends on slip amplitude and exhibits a sharp increase near the transition partial-gross slip.

Nomenclature

E_L	dissipated energy during one hysteresis loop
N	normal load,
T	tangential force
LVDT	Linear Variable Differential Transformer
M152	martensitic stainless steel M152
u	relative displacement

Δu	displacement amplitude
X20Cr13	martensitic stainless steel X20Cr13
COF	Coefficient of friction

2. Materials and Methods

The methodology was based on an experimental analysis performed using the high precision test rig reported in [18], [19]. The general choice of the test parameters developed from the working condition of a shroud of low-pressure blades of steam turbines. Fretting experiments focused on the analysis of the sliding amplitude effects. Tests were performed at room temperature on two stainless steels (M152 and X20Cr13), two nominal contact pressures (25 and 15 MPa), four strokes (10, 15, 20, 50 μm), one heat treatment (quenching – tempering), one frequency (175 Hz) and different test duration (15, 25, 105, 160 million of fretting cycles). The criteria used to choose the test duration was that the accumulated dissipated energy in partial and gross slip regimes were substantially same.

The main peculiarities of the test rig [18], [19] are the free approach of the contact surfaces, high precision displacement control and self-location of the specimens in the same position after assembling-disassembling-assembling operations. Usually, the approach of the contact surfaces in wear and fretting test rigs is rigid. Due to the rigid approach when the mating surfaces are brought in contact, the contact takes place at only one point Fig. **3** (a). Surfaces are kept in contact by the applied normal load. This initial contact point becomes a conformal surface as a consequence of the wear process. Thus, even if two flat surfaces are brought into contact, the nature of the contact is not a flat on flat but is a point contact. In contrast, the kinematics of the free approach of the contact surfaces originates a multi-points contact state (see Fig. **3** (b)).

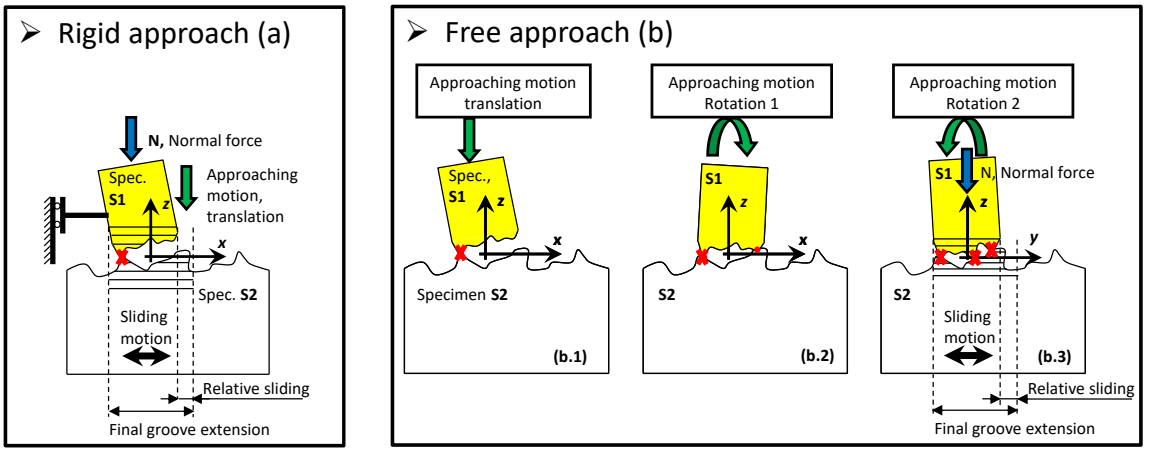

Fig. 3. Rigid versus free approach comparison, ✘ contact points of the mating surfaces.

During the free approach, the contact starts at one point similarly to the rigid approach (Fig. **3** (b.1)) but, in this case, the approaching specimen has two further degrees of freedom, the rotations around the x, y axes. Consequently, the contact takes place at two other points, see (Fig. **3** (b.2), (b.3)). Surfaces are kept in contact by the applied normal load in the center of the specimen.

The specimens are characterized by two sliders with a flat surface of (height 1, width 5.4, and thickness 1 mm) in contact on a common flat surface which has the same width (5.4 mm), Fig. 4 (a). The specimen with two sliders is clamped in a fixture guided by one rod and one arm in order to leave the appropriate degrees of freedom [18], [19]. The arm acts on a load cell that measures the friction force. Its axis is parallel to the sliding direction. The axis of the rod is orthogonal to the sliding direction. This acts on a second load cell that measure the contact force that is orthogonal to the sliding direction. This second measure is used in order to check the quality of the process (e.g. dynamical effects). Excluding the compliance of the test rig components, this specimen has a fixed position. The links rod – fixture – arm – sensors are unilateral hinges. The second specimen (Flat in Fig. 4 (a)) is fixed by a rigid arm to the exciting apparatus. This apparatus is an inertial mass fixed to the ground by means of four springs. A shaker acts on the inertial mass and provides the reciprocating motion [18], [19].

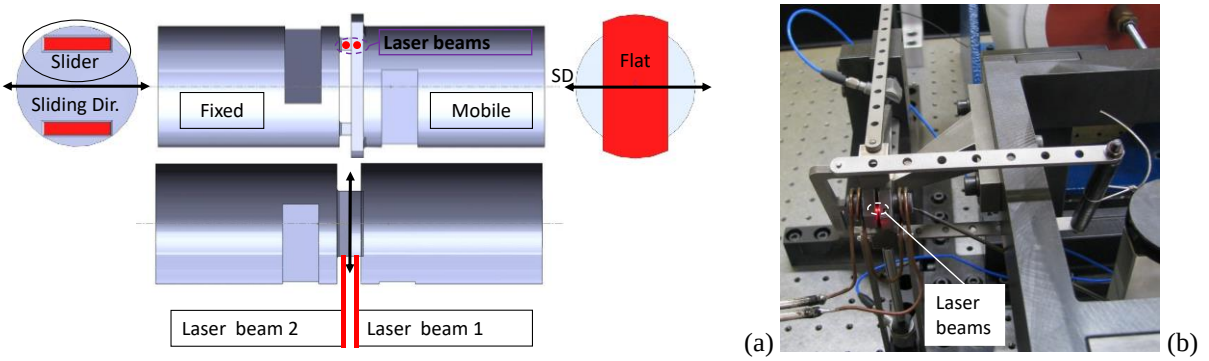

Fig. 4. Specimens: (a) sketch of the fix and mobile specimen (left and right side respectively) with the evidence of the coupling (center side), contact surfaces (red), displacements measurements points (red points), laser beams (red line) and sliding direction (SD); (b) test rig detail of the specimens coupling with the evidence of the displacement measurement points (red points).

The displacements are measured on both specimens close to the contact interface (red points Fig. 4 (a)). These are measured by means of a mirrors system and two laser velocimeter. The relative displacement comes from subtraction and integration of these two velocities. The displacement of the fixed specimen is due to the compliance of the arm and other test rig components. However, this displacement is measured and controlled by relative displacement measure. The test rig control system uses the measurements of the relative displacements in order to regulate the force applied by the shaker to obtain the required imposed relative sliding amplitude of the contact surfaces. It can be concluded that the measure of the relative displacement is not affected by test rig compliances.

The third main characteristic of this test rig is the clamping system of specimens. The system clamps the specimen in only one fixed position. Therefore, the specimens have the same position at each assembly of the test rig. In other words, the contact surface remains the same after assembling-disassembling-assembling operations. Consequently, the wear grooves do not change either. Because of this property, the evolution of the wear can be measured more times on the same couple of mating surfaces. Alignment issues are compensated by the self-aligning properties of free approach. The test procedure used is based on this property and is described by the following main steps:

1. Surface topography measurements of both unworn contact surfaces.
2. Assembly of the test rig.

3. Fretting process with control of the relative displacement for a predetermined number of cycles.
4. Relative displacement, friction force, temperature, hysteresis loops, energy dissipated and other parameters continuously measured during the fretting process.
5. Disassembly of the test rig and cleaning of contact surfaces by means of acetone.
6. Surface topography measurements of worn contact surfaces.
7. Computation of the wear volume.
8. Reassembly and repetition of the steps 2-7 as needed.
9. End of the test.

In the mixed stick-slip regime, the wear volumes are much lower than in gross slip. The measurement of the wear volume plays a fundamental role in order to compare the wear volume that come from these two regimes. In some cases, the wear is just a mild alteration of the roughness profile. Therefore, the wear volume was evaluated with a procedure that takes into account the roughness of the mating surfaces. The detailed procedure is reported in [20]. Wear volumes were measured by comparison of peak and hole volume measurements of asperities at different steps of the fretting process ($V_{p,w}$, $V_{h,w}$ Fig. 5 (a, b)) with peak and hole volumes in unworn conditions ($V_{p,i}$, $V_{h,i}$. Fig. 5 (b)). Peak and hole volumes were measured using a reference plane (Fig. 5 (a)) which was found by means of last square interpolation of unworn area. These points are all points outside the selected areas for volume measurements (rectangular areas with dashed lines in Fig. **5** (b)). A positive wear volume is obtained if the sum of peak volumes decreases and the sum of hole volumes increases. In the case of the sliders, the comparison was made using the entire volume of one slider at each step of the wear process. As a consequence of the two sliders (Fig. 4 (a)) there are two separate contact surfaces subject to the same fretting process. The wear volume of these two couples of contact surfaces were measured independently. This methodology analysis provides an indication of the repeatability of the fretting process.

The friction coefficient (μ) was based on the dissipated energy.

$$\mu = \frac{\boldsymbol{E_L}}{\boldsymbol{4N\Delta u}} \tag{1}$$

Where N is the normal load, Δu is the displacement amplitude of the analysed loop and E_L is the dissipated energy during the same hysteresis loop. The energy loss in one cycle comes from the integral of tangential force T over relative displacement u along the hysteresis loop.

$$E_L = \oint T \, du \tag{2}$$

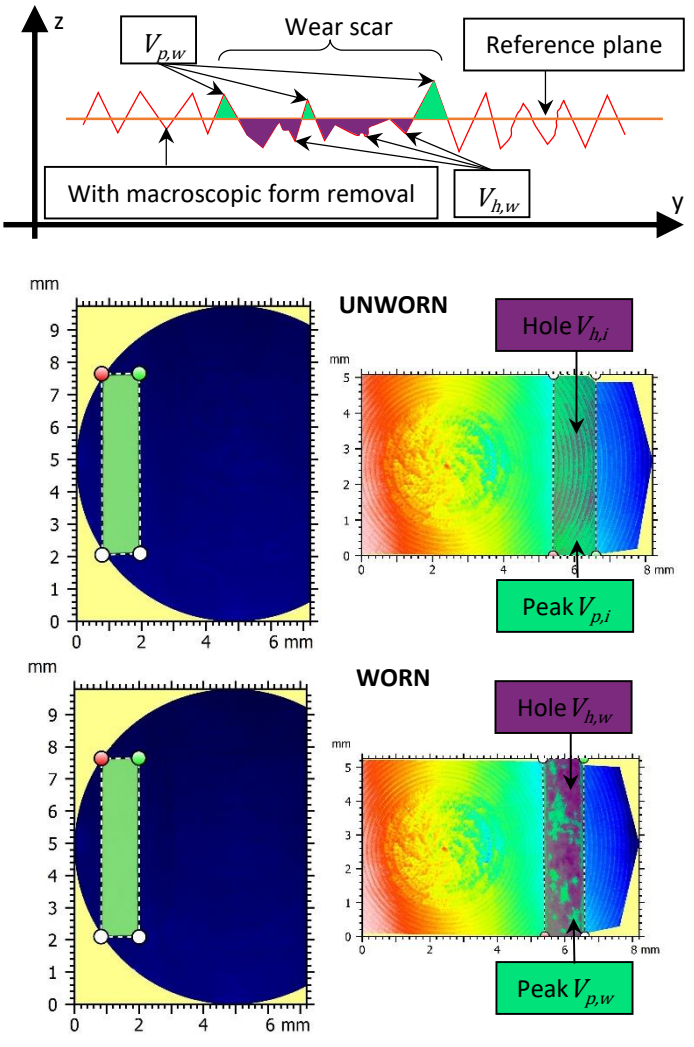

Fig. 5. Wear volume measurements: (a) peak and hole volume definition; (b) peak and hole volume measurement.

The COF energetically equivalent has been chosen in order to have the right value of dissipated energy on the entire relative displacement amplitude. In other words, this COF gives the tangential force equivalent to the tangential force of Amontons-Columbian that should be applied

on the entire stroke. The COF based on this definition cannot be higher than 1. On the other hand, COF obtained by other definitions (e.g. friction force divided by normal load) can be higher than 1. In fretting problem, definitions based on the ratio between measured forces may not preserve the energy dissipation, particularly in partial slip regime. The reason is that fretting hysteresis loops usually display no steady friction force, particularly in partial slip regime. Consequently, the COF definition on a hysteresis loop depends on the property (maximum friction force, average friction force, dissipated energy) that needs to be preserved. The ratio between maximum friction force divided by normal load preserves maximum friction force but not the average friction force and dissipated energy. The adopted definition preserves the dissipated energy and the average friction force on the whole real loop. Moreover, it is also a good methodology for comparing hysteresis loops with different shape. The entire hysteresis loop is represented only by one parameter (COF) that tends to 1 if the shape tends to a rectangle. Vice versa, this will assumes lower values in the case of rhomboidal o elliptical loops.

3. Results

The experimental campaign was based on two quenched and tempered steels at room temperature and frequency of 175 Hz. Table 1 details steels, strokes, normal loads and test duration. The total amount of fretting cycles was 0.665×10^9.

Table 1: experimental project.

ID couple	Material	Stroke, µm	Normal Load, N	Contact Pressure[1], MPa	Cycles, ($\times 10^6$)
#01-01	M152	50	271.8	25	25
#02-05	X20Cr13	50	271.8	25	25
#03-09	X20Cr13	50	163.7	15	15
#04-10	M152	50	163.7	15	15
#05-12	X20Cr13	10	271.8	25	160
#06-13	X20Cr13	20	163.7	15	105
#07-14	X20Cr13	15	163.7	15	160
#08-17	M152	10	271.8	25	160

Common data

Temperature: room temperature

Frequency: 175 Hz

Heat treating: quenching and tempering;

[1] nominal value, normal load/contact surface

Fig. 6 illustrates the evolution of the coefficient of friction (COF) as a function of the number of fretting cycles at the stroke of 50 μm for both steels and both normal loads. The same figure reports the typical hysteresis loops observed during the fretting process. Loops have a parallelogrammatic shape that is substantially stable over the whole fretting processes at the stroke of 50 μm. The loops shape indicates a stable gross slip fretting regime. Loops at low normal load (15 MPa) exhibit a lower friction force than loops at higher normal load (25 MPa). Obviously, the same consideration can be made for the loop areas and dissipated energies.

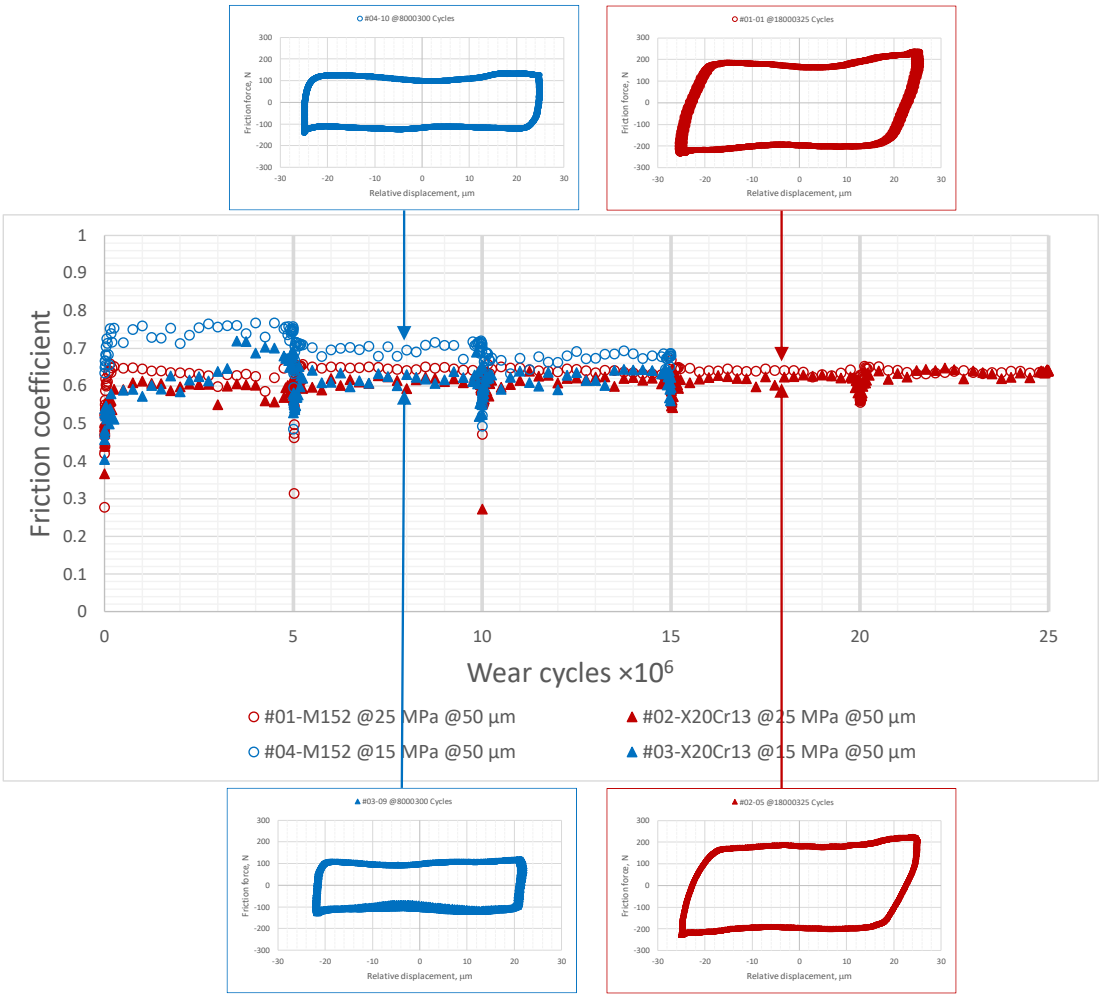

Fig. 6. Friction coefficient as a function of fretting cycles with typical hysteresis loops: gross slip regime, stroke 50 μm, normal load 15 and 25 MPa, M152 and X20Cr13, disassembling – assembling operations at 5×10^6, 10×10^6, 15×10^6, 20×10^6, 25×10^6 cycles.

With regard to the evolution of COF, it should firstly be considered that these fretting processes were stopped each 5×10^6 cycles in order to perform the wear volume measurements.

Consequently, each 5×106 cycles some fast transients (quasi vertical sequences of measurement points, Fig. 6) were observed due to the opening of the contact surfaces and successive operation of disassembling and reassembling. Subsequently to this transient, the global trend was a tendency toward a value of the COF of about 0.62. At the normal load of 25 MPa, the M152 steel showed a COF that is slightly higher than X20Cr13 steel. With the increase of the number of cycles, this difference became less evident and converged to the common value of 0.62 in the last stint ($20\times10^6 – 25\times10^6$ cycles).

At the normal load of 15 MPa, excluding the $3.5\times10^6– 5\times10^6$ cylces stage, the evolution of the COF of X20Cr13 steel was substantially the same as the evolution of this steel showed at the normal load of 25 MPa. Surprisingly, during the $3.5\times10^6 – 5\times10^6$ cylces stage, the COF of X20Cr13 steel at normal load of 15 MPa was higher than at the normal load of 25 MPa. The M152 steel at the normal load of 15 MPa exhibited COF values clearly and surprisingly higher if compared with the same steel at 25 MPa and with all others. This difference remained similar during each stint of 5×10^6 cylces but it decreased when the stint changed. During the last stint ($10\times10^6 – 15\times10^6$ cycles), the values of COF of the M152 steel at the normal load of 15 MPa became similar to the others.

Fig. 7 shows the evolution of COF as a function of the number of fretting cycles at the stroke of 15, 20 μm for X20Cr13 steel at normal load of 15 MPa. In this case, the evolution of COF and hysteresis loops shapes are not stable, as in gross slip regime. Similar results were already observed in [24]. Hysteresis loops change in shape (from parallelogrammatic to rhomboidal and vice versa) and in area. The rhomboidal loops exhibit a characteristic value of COF that is lower than parallelogrammatic loops. Excluding local effects, the shape of loops and characteristic values of COF usually change when the contact is open. At the stroke of 20 μm, shapes of hysteresis loops were essentially parallelogrammatic more or less near to a rectangular shape over the whole fretting process (Fig. 7). The rhomboidal loops at 15 μm were almost located in stages, $60\times10^6 – 95\times10^6$ cycles and $130\times10^6 – 160\times10^6$ cycles (Fig. 7), consequently the percentage of rhomboidal loops was about 47% of the total number of cycles. The change in shape of hysteresis loops suggests a partial slip regime that is more evident at 15 μm than at 20 μm.

Fig. 8 reports the evolution of COF as a function of the number of fretting cycles at the stroke of 10 μm for M152 and X20Cr13 steels at normal load of 25 MPa. At this slip amplitude, the change in shape of the hysteresis loops is more complex than in the previous case. Now the shape switches over three characteristic shapes, parallelogrammatic, rhomboidal and elliptical, and consequently the characteristic values of the COF changes.

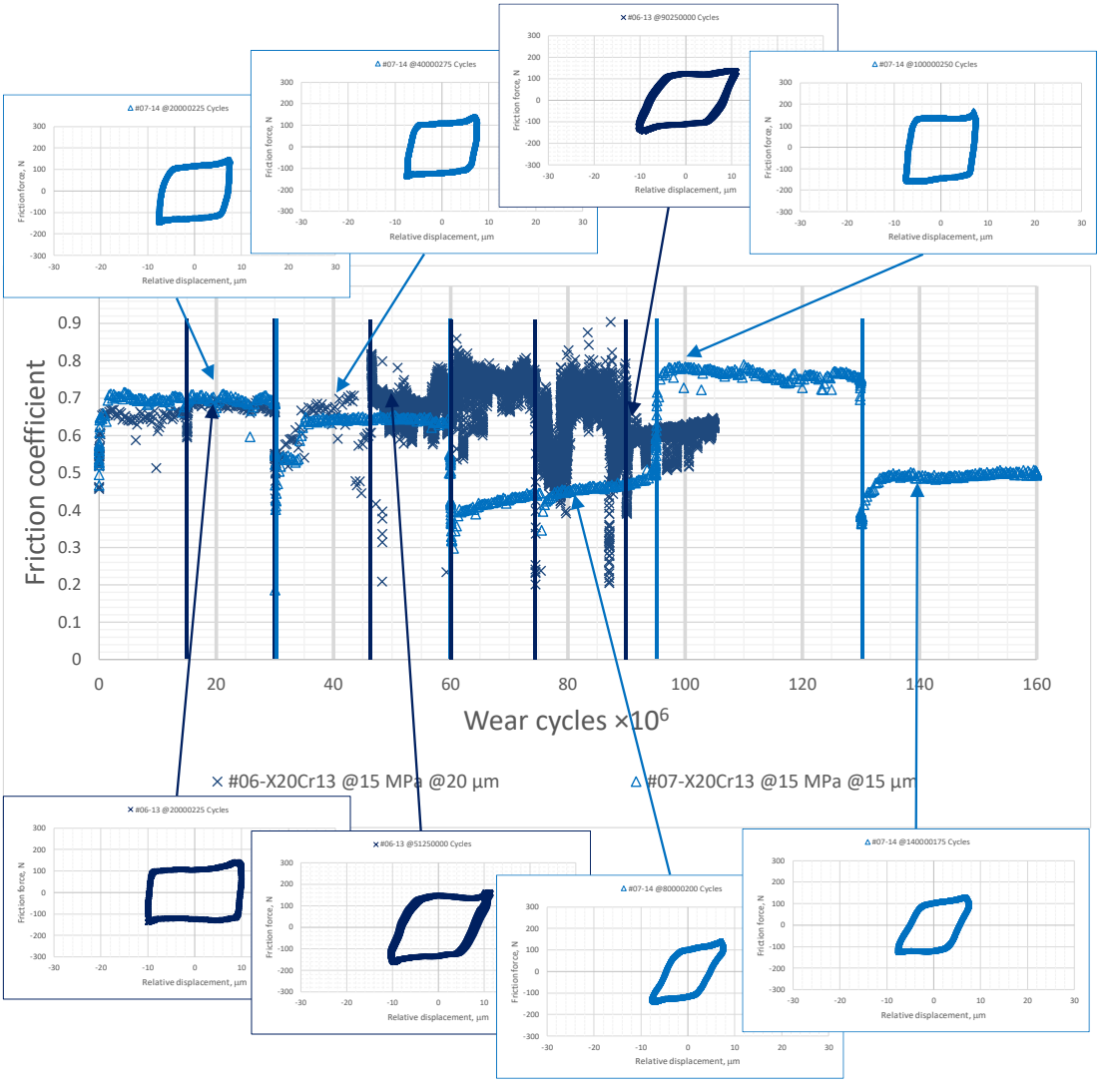

Fig. 7. Friction coefficient as a function of fretting cycles with typical hysteresis loops: gross slip regime, stroke 15, 20 μm, normal load 15 MPa, X20Cr13, disassembling – assembling operations at the vertical straight lines blue and dark blue.

Similarly, to Fig. **7**, if a loop shape switch is observed, this occurs usually when the contact was open for the volume measurements. In the 30×10^6 – 60×10^6 cycles stint of M152 steel (Fig. 8) there is a switch from ellipse to rhombus to ellipse where the rhomboidal loops were observed

between $44.5\times10^6 – 46.5\times10^6$ cycles. For this reason the evolutions of COF of M152 steel is more regular than X20Cr13 steel. The fretting process over this last steel was open more times than M152. Substantially, the X20Cr13 steel exhibits rhomboidal and elliptical loops. The elliptical loops showed a lower characteristic value of COF than the rhomboidal loops. They were almost located in stages, $10\times10^6 – 20\times10^6$; $35\times10^6 – 50\times10^6$; $60\times10^6 – 75\times10^6$ cycles (Fig. 8). The M152 steel was characterised by three shapes elliptical, rhomboidal and parallelogrammatic. Rhomboidal loops where observed during the first two stints $0 – 15\times10^6$ and $15\times10^6 – 30\times10^6$ cycles (Fig. 8) while the elliptical loops were observed during the third $30\times10^6 – 60\times10^6$ cycles stint (Fig. 8). Elliptical loops showed the lowest characteristic values of COF while parallelogrammatic loops showed the highest. Rhomboidal loops displayed intermediate characteristic value of COF. Finally, the fretting regime was stick-slip.

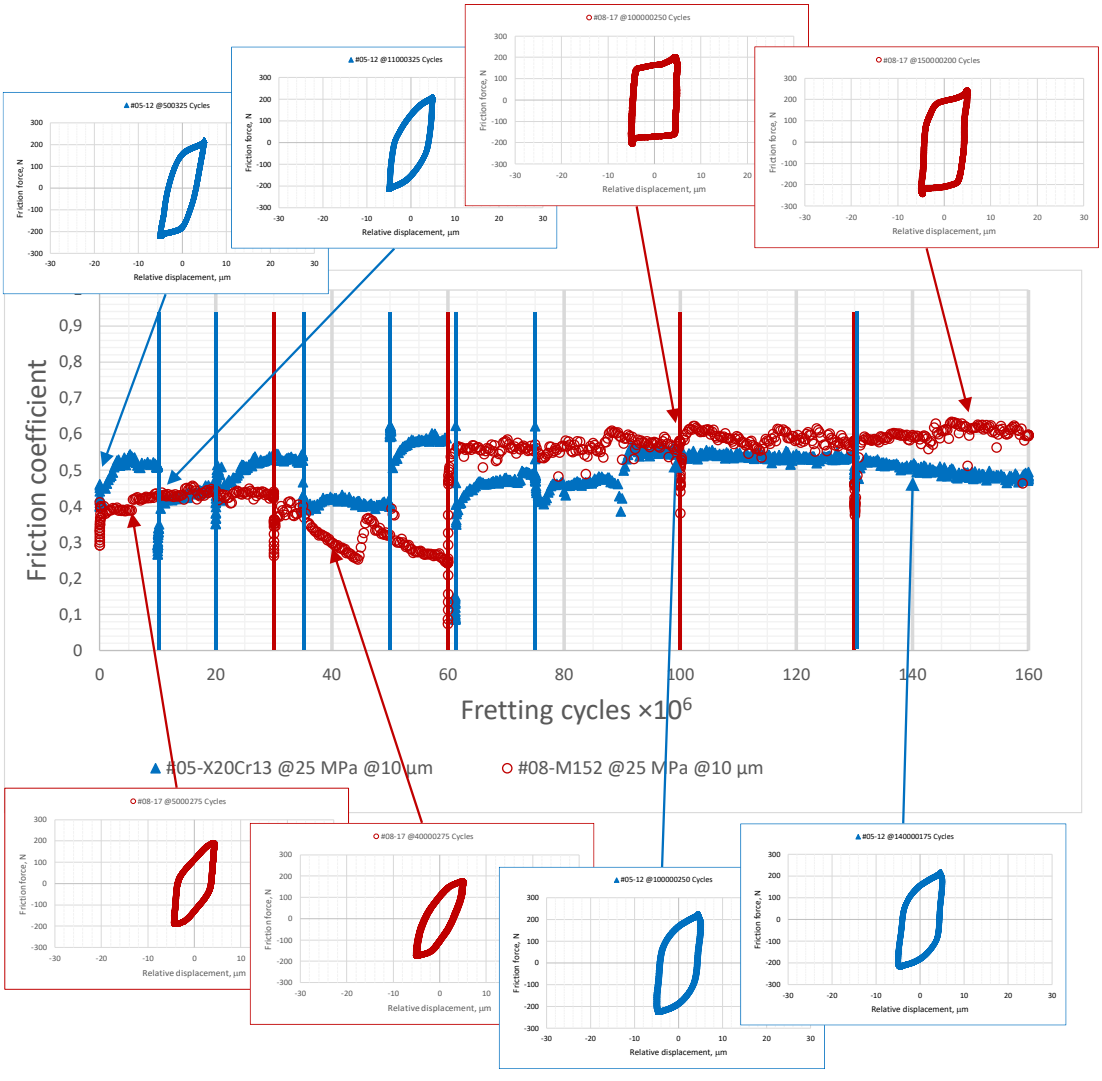

Fig. 8. Friction coefficient as a function of fretting cycles with typical hysteresis loops: gross slip regime, stroke 50 µm, normal load 15 and 25 MPa, M152 and X20Cr13, disassembling – assembling operations at the vertical straight lines blue and red.

Fig. 9 shows total wear volumes (sum of both contact surfaces) as a function of fretting cycles (Fig. 9 (a)) and accumulated dissipated energy (Fig. 9 (b)). At the strokes of 50 µm in gross slip regime, the wear evolution exhibits a linear trend (Fig. 9). In contrast, the trend of wear evolution becomes non-linear in partial slip regime (strokes of 10, 15, 20 µm). These typical characteristic trends are independent of steel type and normal load. Moreover, these trends are displayed in both diagrams, as a function of fretting cycles (Fig. 9 (a)) and dissipated energy (Fig. 9 (b)). The X20Cr13 steel at the stroke of 20 µm exhibited positive wear volume over all measurements and

the evolution shows a sharp non-linearity during the 30×10^6 - 46×10^6 cycles stint (Fig. 9). At strokes of 10, 15 μm both steels evolved initially towards slightly negative wear volumes (increase in volume). Subsequently, they increased and became positive (loss in volume). M152 steel at 10 μm and the X20Cr13 steel at 15 μm substantially exhibits the same evolution (Fig. **9**). It shows slightly negative volumes in 0 – 60×10^6 cycles, increasing towards positive volumes in 60×10^6 – 100×10^6 cycles and it remained substantially constant in the last two stints (130×10^6 – 160×10^6 cycles) The evolution of X20Cr13 steel at 10 μm (Fig. 9) was similar but negative and positive wear volumes were higher. Similar considerations about the wear rate evolution can be made for the diagram wear-energy.

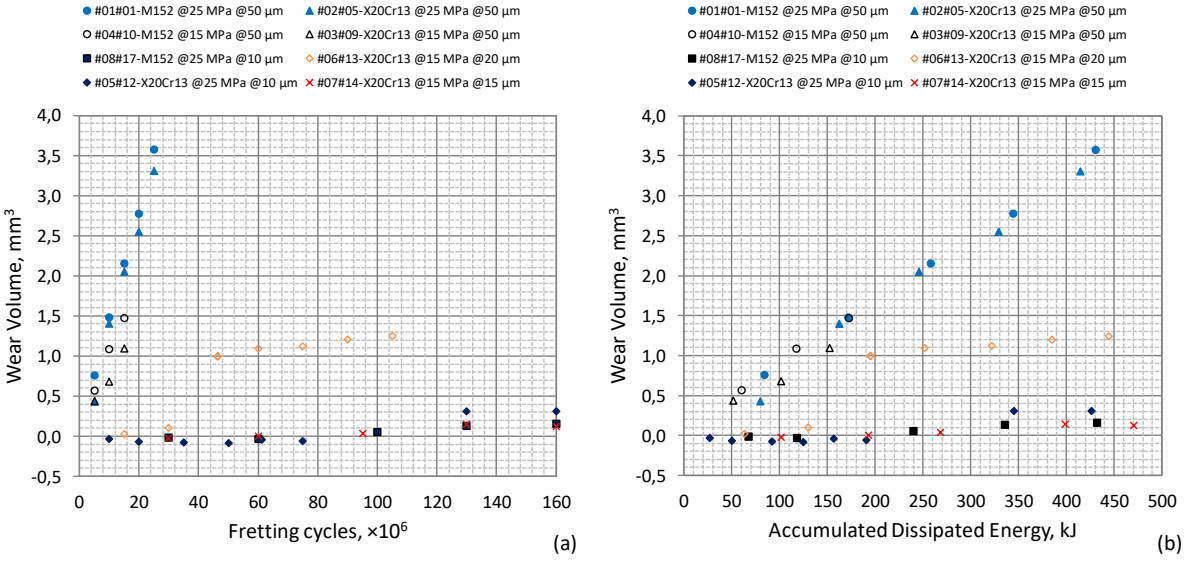

Fig. 9. Wear volumes as a function of fretting cycles (a) and accumulated dissipated energy (b).

With regard to the wear – cycles evolution in gross slip regime (Fig. 9 (a), strokes 50 μm), both steels showed very similar wear rates at higher normal load (25 MPa). At lower normal load (15 MPa), the wear rates were lower than at the higher normal load and there was a difference between the two steels. On the other hand, the wear – energy evolution in gross slip regime (Fig. 9 (b), strokes 50 μm) displayed very similar wear rates for both steel and normal loads. This similarity was less evident only for the couple #03, X20Cr13 steel at lower normal load while the other three cases (couples #01, #02, #04) had substantially the same wear rates.

The wear rates displayed in Fig. 9 are summarized in the amplitude maps reported in Fig. 10. The energy wear rate as a function of the ratio amplitude contact length measured in the sliding direction is reported Fig. 10 (a). The energy wear rates (α) were evaluated by linear interpolation of the wear volume as a function of the accumulated dissipated energy (Fig. 9 (b)). In other words, the energy wear rate is the slope of the linear interpolation of the function volume – energy. The error bar reported for each point is the standard error of the linear interpolation. Fig. 10 (b) reports the average Archard's wear rate coefficient (K) as a function of the ratio amplitude contact length measured in the sliding direction. This coefficient (K) is the ratio between wear volume and Archard's work. This work is the product of sliding distance by normal load. In other words, Archard's wear rate coefficient (K) is the wear volume normalised to the normal load as well as to the sliding distance. This coefficient was evaluated at each number of cycles where the wear volume was measured. The average value was computed using the Archard's wear rate coefficients (K) computed at each normal load and sliding distance (number of cycles) where the wear volumes were measured. The standard deviation of average computing is the error bar reported for each point of Fig. 10 (b). Error bars are reported for each point of both maps. In some cases they are not clearly visible because the magnitude of the error is very small e.g. in gross slip regime. These processes are well described by linear models.

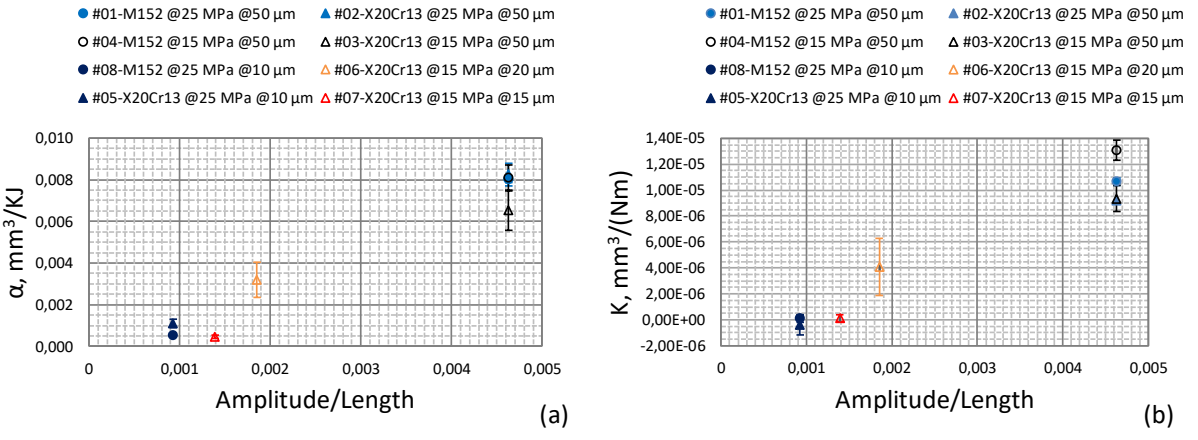

Fig. 10. Amplitude fretting maps in terms of average energy coefficient (a) and average Archard's coefficient (b).

In these maps, circular indicators refer to the M152 steel, while the triangular indicator refer to the X20Cr13. The solid indicators refer to higher normal load while the empties refer to the lower. Colors are associated to one specific stroke. Excluding the gross slip regimes

(Amplitude/length ≈ 0.0046) both maps show a similar evolution. However, the energy map (Fig. 10 (a)) is more independent of the normal load than the map based on Archard's coefficient. The wear rate in partial slip regime is an order of magnitude lower than in gross slip. At end of the partial slip regime, wear rates exhibit a sharp increase. The highest error bar was found at ratio amplitude/length of about 0.00185 (strokes 50 μm, Fig. **10**). The reason is the strong non-linearity of the wear volume evolution (Fig. 9). Consequently, a global average linear model induces strong interpolation error that derives from the sharp non-linearity observed at 46×10^6 cycles.

4. Discussion

The COF in the gross slip regime (at the strokes of 50 μm) seems to converge at a common value of 0.62 (Fig. 6). This indicates that there is no clear evidence of a dependence of the COF on normal load and steel type. Excluding the small stage from 3.5 to 5×10^6 cylces, the COF of the X20Cr13 steel seems to be substantially independent of the normal load (Fig. 6). On the other hand, the M152 steel initially shows a clear dependence of the COF on the normal load. Surprisingly, this dependence is in contrast with the increase of the normal load. However, this dependence becomes much less evident with the increase of the fretting cycles. This can be interpreted as a consequence of the evolution of the contact surfaces. The initial contact surfaces are characterized by a specific morphology and mechanical properties of the asperities. This introduces a dependence of the contact parameters [21] (COF and tangential contact stiffness). This dependence derives from the variation of contact areas of each asperities generated by the variation of morphology, mechanical properties and normal load. In other words, this dependence can origin from a different state of the surface integrity. Even if the fabrication of specimens is the same, machining tool wear or variation of cutting parameters changes the characteristic of contact surfaces in terms of residual stresses and morphology of asperities. For example, [22], [23] illustrate the residual stresses as a consequence of wear tool and cutting parameters. The specimens of the present research were obtained by milling and turning. As a consequence, a small variation of tool feed or a non – appropriate tool wear may have occurred. With the increase of the fretting cycles, the asperities were removed and the contact surfaces

became effectively conformal. Consequently, as of the number of fretting cycles increased, the contact area became less dependent on properties of the asperities than in the initial stage. Moreover, based on third-body theory [25], the morphology of the asperities can also affect the entrapping dynamics of debris between the mating surfaces. This can explain the temporary increase in COF of X20Cr13 steel during the $3.5\times10^6 – 5\times10^6$ cylces stage. Summarizing, in gross slip regime, the COF was independent of two steels and normal load when there were no asperities or when the morphology and mechanical properties of the contact surfaces of asperities were substantially the same. However, in this particular case temporary variation of the coefficient could derive from different dynamics of entrapping-ejection of debris. If a difference of COF comes from different properties of surfaces (morphology and mechanical properties of the asperities), it can be removed by a fretting process adequately long.

The COF in the partial slip regime (Fig. 7, Fig. 8, strokes of 10, 15, 20 μm) showed an much more complex evolution than in gross slip regime. At the stroke of 20 μm (Fig. **7**) the measurements of COF were performed with two different acquisition frequencies. These were lower during the first part of the fretting process ($0 – 46\times10^6$ cylces, Fig. 7) and higher in the second part ($46\times10^6 – 105\times10^6$ cylces, Fig. 7). Moreover, local dynamical effects were extraordinarily frequent in the central part of the process at the stroke of 20 μm ($46\times10^6 – 90\times10^6$ cylces, Fig. 7). The frequency of these effects was much lower in fretting processes at strokes of 10, 15 μm. Interestingly, the COF seems to be more dependent on hysteresis loop shapes than steel type and/or slip amplitude. It should be observed that during the $90\times10^6 – 105\times10^6$ cylces stages at 20 μm (Fig. 7), $30\times10^6 – 60\times10^6$ cylces at 15 μm (Fig. 7), $54\times10^6 – 60\times10^6$ cylces at 10 μm (Fig. 8-X13Cr20) and $60\times10^6 – 160\times10^6$ cylces at 10 μm (Fig. **8**-M152), the loops had a parallelogrammatic shape and the characteristic values of COF was 0.58 – 0.64. Obviously this is excluding local effects, particularly those near to the opening of the contact. In other words, the COF in these stages did not display important differences with respect to the COF for conformal surfaces in gross slip regime (Fig. 6 – strokes of 50 μm). Moreover, in the other parts where hysteresis loops had a parallelogrammatic shape the COF had characteristic values higher than 0.58 – 0.64, similarly to the gross slip regime. These higher values can reach 0.8 and they appear in Fig. 7 and Fig. 8 as higher steps, similarly to the differences found in gross slip regime for not really conformal contact surfaces. Based on this,

the conformity of contact surfaces should be distinguished as formal or real. The formally conformal contact surfaces can exhibit differences in terms surface integrity and morphology of asperities even if they formally have the same shape, e.g. flat on flat. The effectively conformal contact surfaces come from a fretting or wear process long-lasting enough to remove the differences of properties in contact surfaces only formally conformal. With regard to the dynamics of shape change hysteresis loops, the characteristic values of COF for the rhomboidal loop shape were higher than elliptical loops and lower than parallelogrammatic loops. The same relation can be translated in terms of loop areas. This means that the ellipse is contained into rhombus that is contained into parallelogram. Thus, when a monotonical increase of COF is observed, loops switch with a sequence from ellipse to rhombus to parallelogram or a part of this. If an elliptical loops increases its COF, the ellipse became more similar to a rhombus. If rhomboidal loops increase their COF, the rhombus becomes more similar to a parallelogram. When parallelogrammatic loops increase their COF, the shape becomes more similar to a rectangle or it increases the maximum/minimum friction force at the loop extremities. The increase of friction force occurs if there are important wear groove edges along sliding direction [26]. An analogous consideration can made when COF decreases. For example, when an elliptical loop decreases its COF, it reduces the ratio lower/higher axis and become more similar to a line. This dynamics of change in loop shapes is clearly visible in the fretting process of M152 steel at the stroke of 10 μm in the $30\times10^6 – 60\times10^6$ cylces stage (Fig. 8). During the initial half part of this stage, the shape of the loops was elliptical and COF decreased. During the central part, COF increased and the loop shape was rhomboidal. The second half part of the stage was similar to the first: loops were elliptical and COF decreased. This evolution of shape loops as a consequence of amplitude increase is clearly displayed in [19].

In gross slip regime, wear volume evolution as a function of fretting cycles shows an evident dependence on the normal load and steel type (Fig. 9, strokes 50 μm). Wear rate is substantially independent of the normal load and steel type if wear volumes are analysed as a function of the dissipate energy [6]. The tribocouples #01, #02, #04 substantially showed same energey wear rate (Fig. 9 (b)). The tribocouple #03 (Fig. 9 (b) X20C13 steel, 15 MPa) showed a lower wear energy wear rate if compared with #01, #02, #04. This difference could derive from a different state of surface integrity. Surface integrity plays an important role on the wear rate [6]. The

energy map in Fig. 10 (a) accurately summarize this dependence. The tribocouples #01, #02, #04 are substantially overlapped while tribocouple #03 is separate with a partial overlapping of the error bar. The map based on Archard's wear coefficient (Fig. 10 (a)) overlaps the tribocouples #02, #03 (X20Cr13 at different normal load) and distinguish the tribocouples #01, #04 (M152 at different normal load). Taking into account that Archard's wear coefficient assumes a linear dependence on normal load, it should be linear over the X20Cr13 and non-linear over the M152. By an analysis of the wear rete as a function of number of cycles reported in [6], it was concluded that the dependence on the normal load is non-linear. Consequently, in gross slip regime, the energy wear map seems to represent the dependence on the normal load more accurately than the wear map based on Archard' wear coefficient.

The evolution of wear volumes in partial slip regime is non-linear (Fig. 9). Tribocouples #07, #08 (Fig. 9, M152 steel at 10 μm and the X20Cr13 steel at 15 μm) exhibits substantially the same wear volume evolution. Observing only these two couples, it could be stated that the wear volumes are independent of steels, amplitudes and normal loads. If the evolution of tribocouples #05 (Fig. 9, X20Cr13 steel at 10 μm) is introduced in the discussion, this statement seems to be invalidated because #05 shows higher wear volumes. However, an interpretation based on third-body theory [25] is possible. The differences between fretting processes #07 and #08 with respect to process #05 lie not only in process parameters. There is also a difference in number of times when the contact surfaces were opened and closed. They were opened 5 times (number of volume measurements in Fig. 9,) during fretting processes #07 and #08, while process #05 was opened 7 times. Moreover, there is no difference in frequency of contact opening at high number of cycles. This means that process #05 was opened more times than processes #07 and #08 when the third-body was formed (in $0 - 60\times10^6$ Cycle 5 times with respect to 3 of #07 and #08). The third-body of process #05 had been more oxygenated than processes #07, #08. Consequently, the oxidized layers in contact surfaces #05 were higher than in contact surfaces #07 and #08. Thus, a higher wear volume originates by the higher oxidized layer is expected. This explains higher negative values of wear volumes in the initial part of process #05. In the central part of the process, the brittle oxidized starts to break. Higher wear volumes probably derive from higher thickness of oxidized layers. This explains higher positive values of the wear volumes observed in the final part of process #05. Fretting process #06 (Fig. 9, X20Cr13 at the stroke of 20 μm)

shows the strongest and sharpest non-linearity in terms of wear volumes. The increase of non-linearity can be explained with third-body theory, considering that the production and oxygenation of debris increase when the amplitude increase. At the stroke of 20 μm wear volumes showed two differences with respect to the other processes in partial slip (#05, #07, #08) . The first differences is that the non-linearity began much earlier and the second difference is that no negative wear volumes were observed. Beyond 46×10^6 cycles the non-linearity in wear volumes was no longer observed. At same number of cycles, the fretting scar had covered the full contact length in sliding direction (Fig. 11). This suggest that the non-linearity ends when the contact surfaces are effectively and fully conformal.

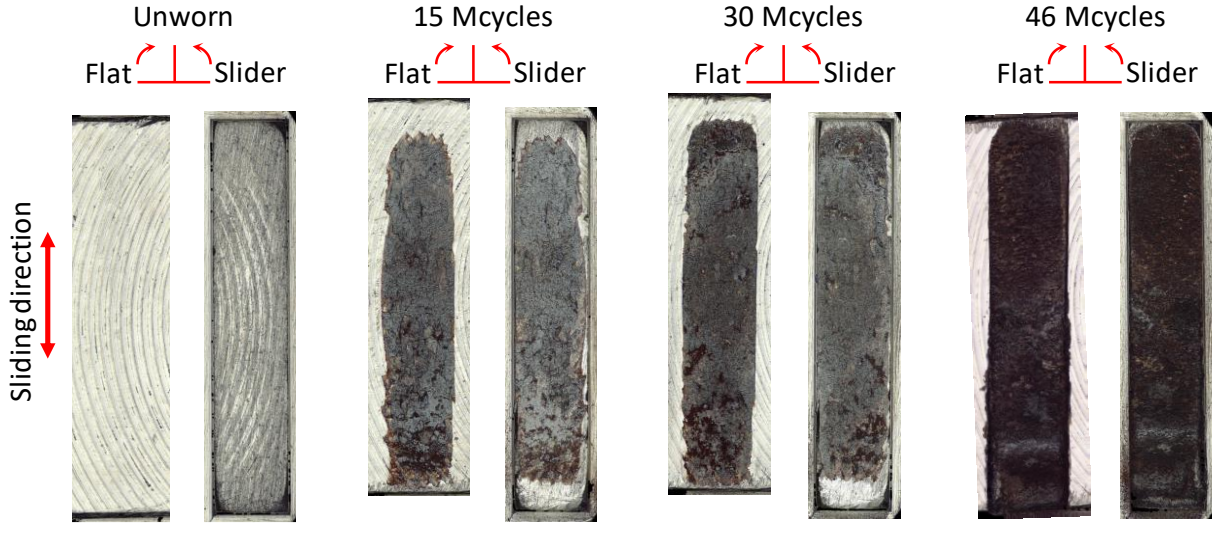

Fig. 11. Fretting scar of X20Cr13 at the stroke of 20 μm.

In this condition, the dynamic of entrapping-ejection of debris can reach a regular state (i.e. a regime). Subsequently to the non-linearity, the wear volumes of X20Cr13 steel at the stroke of 20 μm (#06) evolved linearly. This can be interpreted as an effect of the regime state in dynamics of debris. In [20] negative wear volumes were interpreted as a balance between the generation and ejection of debris. A similar situation can be found in the present research, the generation of debris increased with the increase of the sliding amplitude, while the entrapping and ejection were related to the contact length in the sliding direction. If the contact length increases, the entrapped debris increases while the ejected debris decreases. In this study, the contact length

was constant on all fretting processes while sliding amplitude of the X20Cr13 steel at the stroke of 20 μm was the highest in partial slip regime. The experimental results indicate that at highest stroke in partial slip the volume of ejected debris is higher than the entrapped debries. In contrast, at lower amplitudes, negative volumes were observed until the entrapping process reached a saturation condition.

Based on the fundamental role of the third-body, the amplitude fretting map in Fig. **10** cannot exclude the contact length measured along the sliding direction. The same consideration should also be made for the fretting definition. It should specify what "*low amplitude*" means. Very common definitions is: "*Fretting is the degradation process which occurs on contact surfaces in relative reciprocating sliding motion of low amplitude*". However, "*low amplitude*" should be defined, e.g. *"Fretting is the degradation process which occurs on contact surfaces in relative reciprocating sliding motion of low amplitude with respect to the contact length along the sliding direction*". Obviously, this meaning is clear to fretting specialists but the proposed definition should be straightforward also for non-specialists. Albeit longer. The problem of the fretting definition is not only a formal question. For all specialists, the difference between fretting and reciprocating sliding wear is clear and it was clear also in [11]. However, it is common stated that the border between fretting and reciprocating is at a sliding amplitude of 300 μm, e.g. [11] even if the exact number varies among papers. To assume this border with fixed absolute numerical value is strongly limiting. A paradigmatic process where two contact surfaces which have a contact length along the sliding direction of 100 μm in relative reciprocating motion at the stroke of 100 μm should be subject to fretting. Taking into account that the entire contact area is completely opened at each stroke, these contact surfaces are more probably subject to reciprocating sliding wear. Therefore, the ratio between amplitude and length of contact surface measured along sliding direction must necessarily be taken into consideration.

In partial slip regime, both maps in Fig. 10 show a mild wear at the strokes of 10, 15 μm. At the strokes of 20 μm the maps show a sharp increase in wear rate with a larger error bar. This high error is due to the strongest and sharpest non-linearity observed at this slip amplitude. This non-linearity was found at the ratio between slip amplitude and contact length along the sliding direction of 0.00175. This suggests that the transition from partial slip to gross slip is near and it is associated to a sharp transition in terms of wear rate. This increase in wear rate is in agreement

with the amplitude map in Fig. 1 [11]. A comparison with this map in stick regime does not make sense for real applications. Real mating surfaces can be only formally conformal. Moreover, they can only formally have the same perfectly overlapped contact area. If two mating surfaces that have different contact areas are brought into contact, the contact pressure distribution starts from zero and increases more or less drastically near the border of the lower area [13]. Consequently, if there is an area where the contact pressure goes to zero there is an area where the product of COF by normal load is higher than a non-zero driving force. Obviously, this area could be very small. However, this means that two mating surfaces that have different contact areas are never in stick regime.

5. Conclusion

An experimental analysis was performed based on fretting processes on two steels, two normal loads and different amplitudes. A high precision test rig with free approach of contact surfaces was used. Due the free approach, the contact surfaces were never in point contact condition. The relative displacement measurements were not affected by compliances of test rig components. The wear volumes were evaluated using a procedure that takes into account the roughness effect.

The friction coefficient in gross slip regime was independent of the two steel types and normal load when the contact surfaces were effectively conformal or when the morphology and mechanical properties of the contact surfaces asperities were substantially the same. When the contact surfaces possessed different initial properties, the friction coefficient depended on the normal load during the initial stage of the fretting process. It converged towards a value (about 0.6) that was independent of the normal load if the fretting process was sufficiently long as to remove the asperities, and the contact surfaces became conformal. With similar initial contact surfaces properties, the friction coefficient could show temporary variation due to third-body dynamics, even when it is in contrast with the increase of the normal load. When the initial contact surface properties are different, the initial friction coefficient can be dependent on the normal load, even when it is in contrast with its increase. This dependence can be removed as the contact surface asperities are removed by the fretting process. Thus, the friction coefficient converges to a value that is independent of the normal load if the fretting process lasts long

enough to obtain conformal contact surfaces with the same properties. With regard to the dependence on the steel type it can be concluded that the two similar steels have substantially the same friction coefficient.

The friction coefficient in partial slip regime exhibited less stable evolution than in gross slip regime. This was more influenced by the shapes of the hysteresis loops than steel type and sliding amplitude. Parallelogrammatic loops exhibited substantially the same friction coefficients (about 0.6) at all amplitudes and for both steels when there were stable and conformal contact surfaces. The change in loop shapes usually were found near the opening of the contact surfaces. Characteristic values of the friction coefficient exhibits higher oscillation than in gross slip regime when the contact surfaces were not effectively conformal. With regard to the dynamics of change in loop shape, the characteristic value of friction coefficient for the elliptical loop shape was lower than for rhomboidal loops and these were lower than parallelogrammatic loops. This means that the ellipse is contained in the rhombus and the rhombus is contained in the parallelogram. Thus, when friction coefficient increases monotonically, loops switch with an ellipse – rhombus – parallelogram sequence or a part of this. If the friction coefficient of elliptical loops increases, the ellipse becomes more similar to a rhombus. If the loop shape is rhomboidal, the rhombus becomes more similar to a parallelogram. Conversely, if the loop shape is parallelogrammatic, it becomes more rectangular or it increases the maximum/minimum friction force at the loop extremities. This occurs if there are important wear groove edges along sliding direction. An analogous consideration can be made when the friction coefficient decreases. If the loop shape is elliptical, the ellipse reduces the ratio lower/higher axis and becomes more similar to a line. The properties of contact surfaces plays a fundamental role on friction, and this is discussed in the present paper in terms of morphology asperities and surface integrity. The concept of formal and effectively conformal contact surfaces is proposed. The effectively conformal contact surfaces derive from a fretting or wear process that lasts long enough to remove the differences of properties in contact surfaces only formally conformal. A formally conformal contact surfaces can exhibit differences in terms of surface integrity and morphology of asperities.

The evolution of wear volume exhibits a linear trend in gross slip regime and a non-linear trend in partial slip. The strongest and sharpest non-linearity occurs near the transition partial-gross slip. Moreover, the non-linearity ends when the wear scar covers the whole contact length

along the sliding direction, i.e. when the contact surfaces are really and fully conformal. These volume evolutions cannot be interpreted without considering third-body, wear scar evolution and properties of contact surfaces (asperities and surface integrity). Consequently, the contact length measured along the sliding direction plays a fundamental role. Therefore, wear rates are summarized in two maps as a function of amplitude normalized with respect to the contact length measured along the sliding direction. The wear rates are based on the dissipated energy and Archard wear coefficient. By comparing these two maps it can be concluded that the energy map provides a more accurate description in gross slip regime. Both maps exhibit an increase of error near the transition partial-gross slip due to the stronger and sharper non-linearity in wear volume evolution. In partial slip regime at low ratio amplitude length, the wear rate seems to be independent of slip amplitude and steel type. On the other hand, wear rate is dependent on the number of times that the contact has been opened. By contrast, wear rate exhibits a sharp increase at higher ratio amplitude length (near the partial-gross slip transition).

Future research should include model to support experimental analysis, better define and verify the sharp increase in wear near the partial-gross slip transition. Depending on the results of detailed study of this transition, the gross slip reciprocating transition also should be analysed.

References

[1] E.M. Eden, W.N. Rose, F.L. Cunningham, Endurance of metals, Proceedings of the Institute of Mechanical Engineers 4, (1911**)** 839-974.

[2] R. B. Waterhouse, A historical introduction to fretting fatigue. In Helmi Attia, M., Waterhouse, R. B., (Eds.), Standardization of Fretting Fatigue Test Methods and Equipment, (ASTM STP 1159), American Society for testing and Materials: Philadelphia, Pennsylvania, USA, 1992; pp. 8–9, ISBN-EB: 978-0-8031-5214-4, DOI: 10.1520/STP1159-EB.

[3] G.A. Tomlinson, The rusting of steel surfaces in contact, Proceedings of the Royal Society of London, Series A, 115, (1927) 472-483.

[4] M. Lavella, D. Botto, Fretting Fatigue Analysis of Additively Manufactured Blade Root Made of Intermetallic Ti-48Al-2Cr-2Nb Alloy at High Temperature, Materials 11, (2018**)** 1052. DOI: 10.3390/ma11071052

[5] S. Fouvry, C., Paulin, S. Deyber, Impact of contact size and complex gross-partial slip conditions on Ti-6Al-4V/Ti-6Al-4V fretting wear, Tribol. Int. 42, (2009) 461–574. DOI: 10.1016/j.triboint.2008.08.005

[6] Lavella, M.; Botto, D. Fretting wear of alloy steels at the blade tip of steam turbines, Wear, 426-427, (2019**)** 735–740. DOI: 10.1016/j.wear.2019.01.039

[7] T.J. Carter, Common failures in gas turbine blades. Eng. Fail. Anal. 12, (**2005)** 237-247

[8] C.M. Firrone, M. Allara, M.M. Gola, A contact model for nonlinear forced response prediction of turbine blades: Calculation techniques and experimental comparison, Proceedings of the ASME Turbo Expo, Berlin, Germany; 9 June, 9-15 2008 Abstract Number.

[9] C. M. Firrone, T. Berruti, M.M. Gola, On force control of an engine order-type excitation applied to a bladed disk with underplatform dampers, Journal of Vibration and Acoustics, Transactions of the ASME 135 (2013) 041103, DOI: 10.1115/1.4023899.

[10] C. Gastaldi, A. Fantetti, T.M. Berruti, Forced response prediction of turbine blades with flexible dampers: The impact of engineering modelling choices, Applied Sciences 8, (2017**)** 34. DOI: 10.3390/app8010034.

[11] O. Vingsbo, S. Söderberg, On fretting maps, Wear 126, (1988) 131–147.

[12] S.C. Lim, M.F. Ashby, Wear-Mechanism Maps, Acta metal. 34, (1987) 1–24. DOI: 10.1016/0001-6160(87)090209-4

[13] D. Botto, M. Lavella, A numerical method to solve the normal and tangential contact problem of elastic bodies, Wear 330-331, (2015) 629–635. DOI: 10.1016/j.wear.2015.02.046

[14] J. Madge, S. Leen, I. McColl, P. Shipway, Contact-evolution based prediction of fretting fatigue life: effect of slip amplitude, Wear 262 (9-10) (2007) 1159–1170

[15] J. Knudsen, A.R. Massih, Evaluation of fretting wear data with the aid of mechanism-maps, 18th International Conference on Structural Mechanics in Reactor Technology, SMiRT 18, Beijing, China, 7–12 August 2005, 2690-2703

[16] S.R. Pearson, P.H. Shipway, Is the wear coefficient dependent upon slip amplitude in fretting? Vingsbo and Söderberg revisited, Wear 330-331 (2015) 93–102.

[17] S. Fouvry, P. Kapsa, L. Vincent, Analysis of sliding behavior for fretting loadings: determination of transaction criteria, Wear 185 (1995) 35–46.

[18] M. Lavella, D. Botto, M.M Gola, Test rig for wear and contact parameters extraction for flat-on-flat contact surfaces, ASME/STLE 2011 International Joint Tribology Conference, IJTC 2011, Los Angeles, CA, United States, 24-26 October 2011, DOI: 10.1115/IJTC2011-61234.

[19] M. Lavella, D. Botto, M.M. Gola, Design of a high-precision, flat-on-flat fretting test apparatus with high temperature capability, *Wear* 302 (2013) 1073–1081, DOI: 10.1016/j.wear.2013.01.066.

[20] M. Lavella, Contact Properties and Wear Behaviour of Nickel Based Superalloy René 80, Metals 6 (7) (2016) 159, DOI: 10.3390/met6070159.

[21] D. Botto, M. Lavella, High temperature tribological study of cobalt-based coatings reinforced with different percentages of alumina, Wear 318, (2014) 89–97. DOI: 10.1016/j.wear.2014.06.024

[22] T. Berruti, M. Lavella, M.M. Gola, Residual stresses on Inconel 718 turbine shaft samples after turning, Machining Science and Technology 13 (2009) 543–560, DOI: 10.1080/10910340903451472.

[23] M. Lavella, T. Berruti, E. Bosco, Residual stress analysis in Inconel 718 milled turbine disk, International Journal of Machining and Machinability of Materials 4 (2008) 181–194, DOI: 10.1504/IJMMM.2008.023193.

[24] Z.R. Zhuo, L. Vincent, Mixed fretting regime, Wear 181-183, (1995) 531–536.

[25] M. Godet, The third-body approach: a mechanical view of wear, Wear 100, (1984) 437–452.

[26] M. Lavella, D. Botto, Fretting wear characterization by point contact of nickel superalloy interfaces, Wear 271, (2011) 1543-1551. DOI: 10.1016/J.wear.2011.01.064